LASER INTERFEROMETER GRAVITATIONAL WAVE OBSERVATORY
- LIGO -
CALIFORNIA INSTITUTE OF TECHNOLOGY
MASSACHUSETTS INSTITUTE OF TECHNOLOGY

Technical Note	LIGO-T2500248-v1	05/15/2025

2025 LIGO SURF Interim Report 2: Mapping and Correcting the Surface of the GQuEST End Mirrors

Rafael C. Volkamer-Pastor

California Institute of Technology
LIGO Project, MS 18-34
Pasadena, CA 91125
Phone (626) 395-2129
Fax (626) 304-9834
E-mail: info@ligo.caltech.edu

Massachusetts Institute of Technology
LIGO Project, Room NW17-161
Cambridge, MA 02139
Phone (617) 253-4824
Fax (617) 253-7014
E-mail: info@ligo.mit.edu

LIGO Hanford Observatory
Route 10, Mile Marker 2
Richland, WA 99352
Phone (509) 372-8106
Fax (509) 372-8137
E-mail: info@ligo.caltech.edu

LIGO Livingston Observatory
19100 LIGO Lane
Livingston, LA 70754
Phone (225) 686-3100
Fax (225) 686-7189
E-mail: info@ligo.caltech.edu

http://www.ligo.caltech.edu/

Abstract

The GQuEST (Gravity from the Quantum Entanglement of Space-Time) end mirrors are susceptible to surface deformations which can cause incomplete interference at the differential output. I used an optical profiler to image the surface of these end mirrors and calculated the coupling coefficients to higher order modes. Using a custom adjustable mirror mount, I was able to actuate on the end mirrors and correct for these deformations. We expect to need to correct 2.6×10^{-4} diopters of focusing power and I have been able to correct 9.4×10^{-2} diopters, thus enabling GQuEST to lower the classical noise floor by minimizing the mirror thickness while minimally increasing the contrast defect. This correction involved a mixture of the HG_{02}, HG_{11}, and HG_{20} modes. I expect to improve the precision and purity of my corrections with a more direct mounting system I recently installed.

1 Introduction

The study of quantum gravity aims to find a joint theory of gravitation and quantum mechanics. Substantial theoretical efforts have been made toward quantum gravity. Erik Verlinde and Kathryn Zurek predict 'geontropic' fluctuations, stochastic fluctuations of space-time geometry induced by entropy [1]. GQuEST (Gravity from the Quantum Entanglement of Space-Time), an experiment in the McCuller Lab at Caltech, aims to test this theory by analyzing the phase of light. When light propagates through a space with these fluctuations, it is predicted to accumulate a phase difference relative to light traveling without the fluctuations. The goal of GQuEST is to detect these geontropic fluctuations using a tabletop Michelson interferometer, refer to Figure 1.

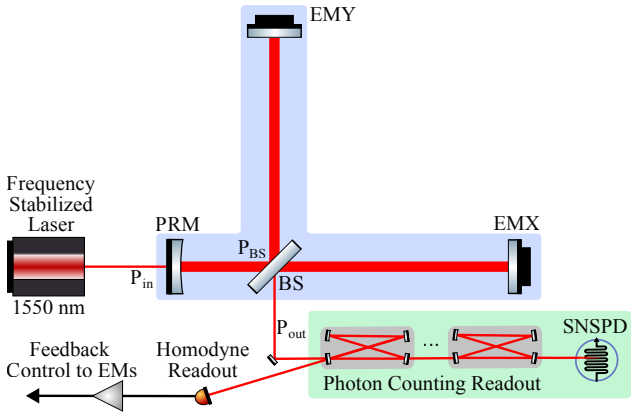

Figure 1: Michelson Interferometer used in GQuEST setup [2].

Geontropic fluctuations are characteristically of very low amplitude, roughly 7 orders of magnitude below the quantum shot noise of a lab scale, high power interferometer. Hence, to get strong results (5σ significance test), experiments are expected to take a run time of around 6 months [2]. Although feasible, this duration can be reduced by using the new photon-counting technique proposed by GQuEST. The method aims to filter the output

light such that only photons carrying the signal are detected; however, some noise will still pass. An advantage to this new method is that it is not quantum limited, unlike the traditional homodyne readout of interferometers. This drastically reduces the total noise to 1 order of magnitude above the signal (compared to the previous 7), causing classical noise, for example vibrations in optical components, to become the new bottleneck. The photon counting method is expected to get strong results (5σ significance test) in weeks, compared to 6 months with traditional homodyne readout [2].

2 Objective

This project focuses on the consequences of reducing classical noise for the GQuEST end mirrors and the resulting necessary modifications. The contribution to the noise floor from the substrate of the mirror can be approximated by the following analytical equation,

$$\bar{S}_L^{SMN}(\Omega) = \frac{16 k_B T h \varphi_s}{\pi^3 M_s w^2 \Omega} \tag{1}$$

where k_B is Boltzmann's constant, T is temperature, h is mirror thickness, φ_s is the mechanical loss angle of substrate, M_s is the P-wave modulus of substrate, w is beam width (2σ radius in intensity), and Ω is measurement angular frequency [2]. It is easier to modify the mirror thickness than the temperature of the interferometer to reduce noise. Hence, GQuEST plans to utilize 2 mm silicon mirror, making the noise floor from the substrate below the coating thermal noise floor which we have less control over.

However, minimizing the mirror thickness causes the mirror to be more pliable. The GQuEST mirrors are made out of a substrate with a highly reflective Bragg reflection coating, similar to LIGO's mirrors. When the coating is applied it curves the face of the mirror as described,

$$r_{curv} \approx \frac{E_s h^2}{6\sigma_c h_c (1 - v_s)} \tag{2}$$

where E_s is Young's modulus of the substrate (the stiffness of the mirror), h is mirror thickness, σ_c is the coating stress, h_c is the thickness of the coating, and v_s is the Poisson ratio for substrate. With the current proposed parameters for GQuEST, $r_{curv} \approx 7.6$m [2]. Hence, it is clear that although minimizing the mirror thickness (h) is beneficial for reducing classical noise it results in a sharper mirror curve, the consequences of which I will further explain in the following paragraph.

When light reflects off of a curved mirror surface some of the light is converted into higher-order modes (HOMs). If the mirrors are not curved identically the HOMs will not all destructively interfere and hence produce a contrast defect, which causes extra light to escape the interferometer, increasing the 'bad' photon rate (photons passing the filter due to

imperfections and not geontropic fluctuations). The optical power loss of these modes can be estimated to be roughly $D = 2/r_{curv}$. Specifically, a difference in the end-mirror curvature on the X and Y arms of the interferometer would scatter the majority of the light into the (Hermite-Gauss) HG_{20} and HG_{02} modes. The current hope is that these will be the only significant modes we need to correct for.

The amplitude coefficients of these modes would be

$$K_{20} \approx \frac{kD_x w^2}{4\sqrt{2}},\ K_{02} \approx \frac{kD_y w^2}{4\sqrt{2}} \tag{3}$$

where $D_x = D_x^{EMX} - D_x^{EMY}$ and $D_y = D_y^{EMX} - D_y^{EMY}$. This scattered light creates a contrast defect of $\Lambda_{CD} = K_{20}^2 + K_{02}^2$. Therefore, to achieve a significantly low contrast defect ($\Lambda_{CD} < 10$ppm) total curvature mismatch needs to be $D_{tot} = \sqrt{D_x^2 + D_y^2} < 3\times10^{-4}$ diopters. With the current proposed parameters for GQuEST the mirror mismatch is expected to be roughly 0.26 diopters, indicating that there will need to be some curvature correction method [2].

We will initially compensate by coating the back of the mirror with an anti-reflective coating of custom thickness to cancel as much of the induced curvature as possible. An additional approach is to try to match the curvature of the two end mirrors in hopes to cancel out the HOMs. However, it likely we can't find perfect pairs and hence should not rely on their destructive interference. Instead, the remainder of the curvature difference will be adjusted through a custom mirror mount that is designed to twist and bend the mirror to counteract the curvature induced by the coating stress.

The goal of this project is to develop and test different methods to correct the curved surface of the GQuEST end mirrors to enable the photon counting method as a tool to study quantum gravity. Specifically, the focus of this summer will be to generate pure and combinations of HOMs under the assumption that if we learn how to generate HOMs in a consistent fashion then we will be able to make an inverse adjustment to remove them in the future. The success of this overarching goal is determined by our ability to generate individual and complex mixtures of both astigmatic modes and the defocus mode, a visual representation can be seen in figure 2. This work builds on a previous project by LIGO SURF student Erin McGee, who worked under the mentorship of Daniel Grass during the summer of 2024; the current project will serve as a continuation of her efforts and will also be mentored by Daniel Grass.

Some intermediate objectives include becoming familiar with the mirror mounts seen in figure 3, developing an adjustment to the mount to generate the defocus mode, testing the maximum stress threshold, and developing a simulation to predict what modes different mirror surfaces will generate.

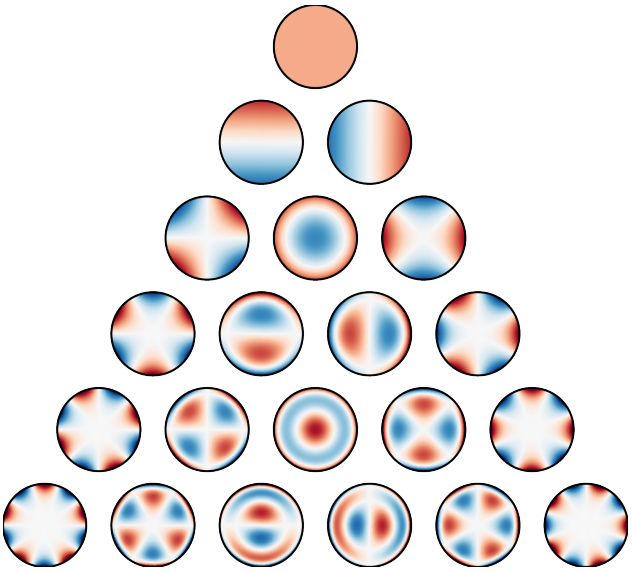

Figure 2: Visualization of the Zernike Polynomials made by Nschloe [3]. The Zernike polynomials provide an orthogonal basis on the unit disk. The top most mode refers to a mirrors position on the z-axis. The two modes in the second row refer to the tip and tilt of the mirror. The defocus mode is the middle mode of the third row (O mode). The astigmatic modes are the leftmost and rightmost mode in the third row (Twist and X Mode).

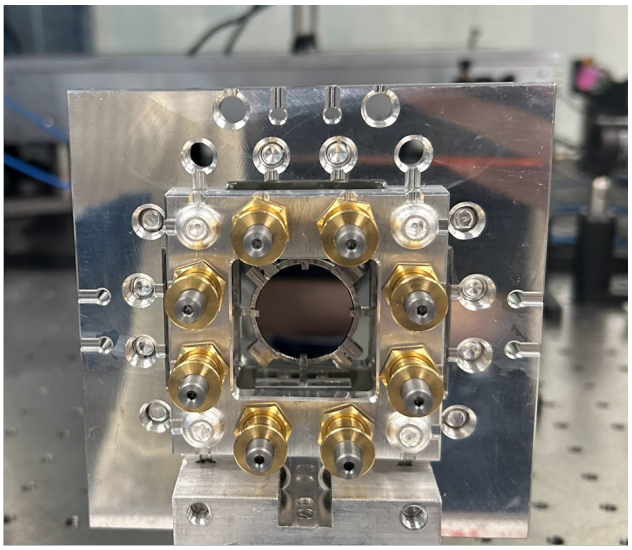

Figure 3: Image of the GQuEST mirror mount. In the image we see the 8 adjustment screws on the back of the mirror. There are an addition 4 adjustable screws on the front side oriented in a plus shape.

3 Approach and Current Achievements

3.1 Mirror Surface and Deformations

This project uses a NanoCam HD, a small scale optical profiler, as its primary measurement apparatus. The profiler can take surface measurements of the mirror to within an angstrom. This allows us to calculate the curvature of the unstressed mirror and observe how the mirror surface reacts to adjustments from the mount. The end mirror and NanoCam have been set-up and are able to record data.

The mirror sits in a mount with 12 adjustment screws, figure 3. The screws put tension on small rods attached to the side of the mirror, the bending of these rods causes the mirror to deform.

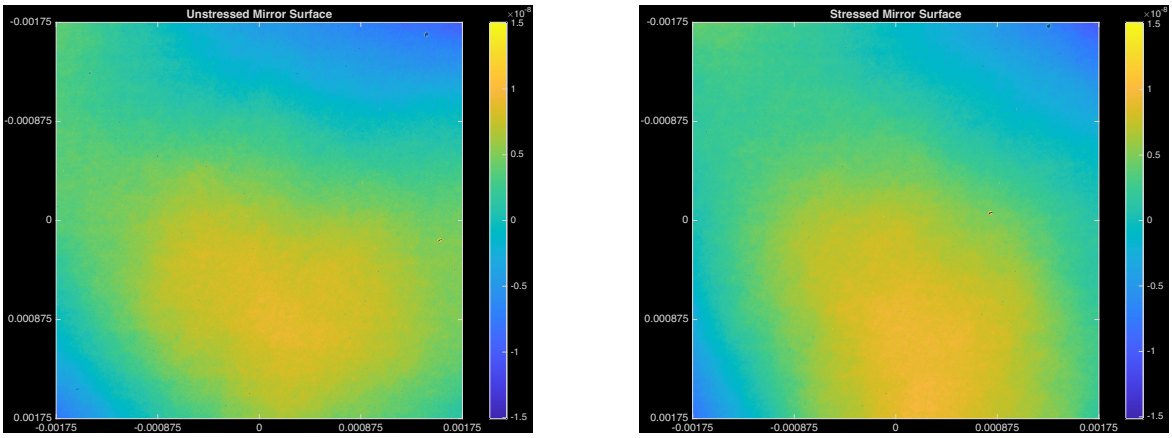

(a) Unstressed Mirror (b) Stressed Mirror

Figure 4: Unstressed and Stressed mirror for Xmode. Attempting to create an Xmode (rightmost mode on the third row of figure 2). This is achieved by engaging the left and right screw on the front side of the mirror mount, and engaging the top and bottom set on the bottom of the mount.

As can be seen in figure 4 the deformations in the unstressed mirror overpower any corrections by the mirror mount. These baseline deformations are caused by the circular housing that the mirror sits in. This housing puts tension on the mirror to hold it stable. A more insightful image to analyze how the mirror mount deforms the mirror surface is the delta between the stressed and unstressed mirror, figure 5.

By looking at the difference between the stressed and unstressed mirror we are able to more clearly see that we are creating the Xmode (rightmost mode on the third row of figure 2) that we were aiming for. The next set of objectives is to generate the defocus and plus mode, see how much we are able to deform the mirror, and try to find a way to avoid any baseline tensioning while still holding the mirror stable.

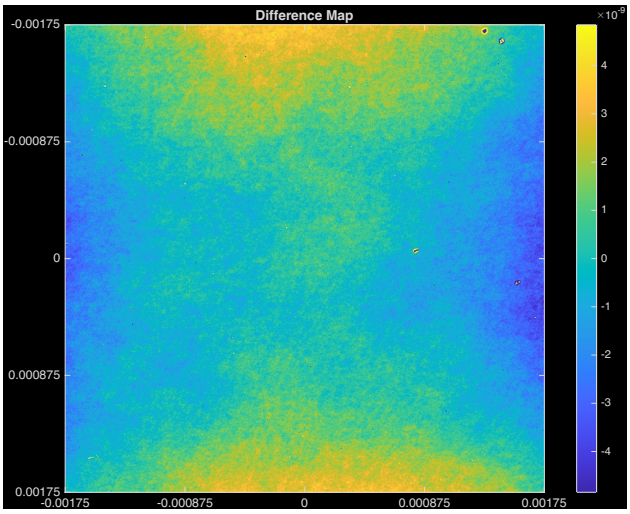

Figure 5: Difference Map for Xmode. The difference between the unstressed mirror 4a and the stressed mirror 4b when trying the generate the Xmode. The difference was calculated stressed minus unstressed.

3.2 Coupling Coefficients

I have also developed a simulation in MATLAB which takes the data from the optical profiler and calculates the coupling coefficients to higher order modes.

The code calculates these coefficients using the following two equation. This tells us how much of the incoming beam is contained in the outgoing beam,

$$k_{nmn'm'} = \int\int u^*_{n'm'} e^{2ik\tilde{z}(x,y)} u_{nm}(x,y)dxdy \tag{4}$$

where k is the laser wave number, $\tilde{z}(x,y)$ is the surface of the mirror, and u_{nm} is a function of the beam and the relevant modes given by,

$$\begin{aligned} u_{nm}(x,y) = \left(\frac{1}{2^{n+m-1}n!m!\pi}\right)^{1/2} \left(\frac{1}{w_0}\right)\left(\frac{q_0}{q(z)}\right)\left(\frac{q_0 q^*(z)}{q^* q(z)}\right)^{(n+m)/2} \\ \cdot H_n\left(\frac{\sqrt{2}x}{w(z)}\right) H_m\left(\frac{\sqrt{2}y}{w(z)}\right) e^{-ik\frac{(x^2+y^2)}{2q(z)}} \end{aligned} \tag{5}$$

where n and m refer to the Hermite–Gaussian modes HG_{nm}, w_0 is beam waist, $w(z)$ is the beam width, q is the complex beam parameter, x and y are the transverse directions of the beam, z is the beam axis, and H is the Hermite Polynomial of corresponding order n or m [4]. This simulation will be necessary to verify that our mirror mount is influencing the wavefront in the desired fashion.

There is a major limitation with the NanoCam, with the current set of objectives we are only able to capture a 3.5 mm by 4.5 mm area. The 2σ power radius of the laser on the mirror is expected to be around 3 mm which means the area the NanoCam images does not fully encompass the laser beam. Not only is there missing power but additionally the Hermite Polynomials are not orthogonal on such a small scale. This means that the coupling coefficients calculated from this limited area will overlap and can't just be scaled up to full power.

3.3 The Zernike Approach

The first approach I took to deal with the limited field of view of the NanoCam was to approximate more of the mirror area. The Zernike Polynomials feel like a natural choice as they are an orthogonal basis on the unit circle. I fit a restricted domain of the Zernike Polynomials to the NanoCam data and then plot those coefficients on the full unit circle. Expanding to a wider domain leads to more of the beam being included in the mirror surface, this improves the coupling coefficient calculations in two ways. Firstly we are able to approximately include the entire beam power in the calculations and secondly the Hermite Polynomials get closer to being orthogonal as we expand the mirror surface.

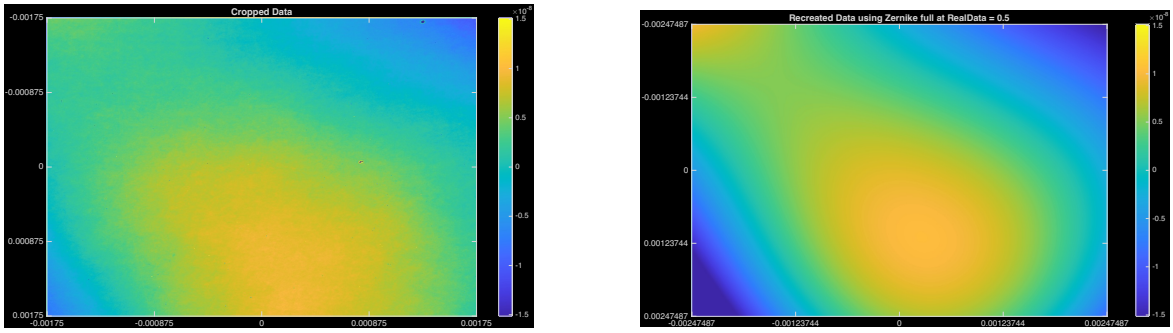

(a) Raw Data from NanoCam (b) Expanded Data with Zernike (2x)

Figure 6: In figure 6a we can see a height map of the mirror surface. This is the raw data from the NanoCam. In figure 6b we can see the expansion of this data using Zernike Polynomials up to degree 3. In this example I doubled the area of the mirror.

I learned, however, that there are numerous limitations with this approach. As we increase the expansion of the mirror surface we fit the Zernikes on a smaller subset of the unit circle. On these smaller domains the Zernike polynomials are no longer orthogonal and look more and more alike. This leads to more error in our expansions. To measure the error in the expansion I looked at the difference between the overlapping region of the expanded and raw data. The rms of this difference map was greater than than the rms of the raw data with any expansions greater than 2x. Due to this high error I have discarded the Zernike approach.

3.4 Least Squares Fit and Image Stitching

The current approach is use a combination of more imaging area, a least squares fit, and the matrix approach to calculate our coupling coefficients. Due to the geometry of the profiler and mirror mount we only have the ability to scan the mirror in the y-direction. By mounting the mirror on a two axis stage we can image a total area of 4 mm $\times$ 7.5 mm area. The NanoCam is only able to capture 4 mm $\times$ 3.5 mm area at a time. To create the larger image I took three vertically stacked images with roughly 1.5 mm of overlap and stiched them together. The NanoCam needs to refocus onto the mirror surface for each image and this involves a piston, tip, and tilt adjustment. I assume that the mirror surface should be the same in the overlapping regions and hence can calculate and correct for the refocusing of the NanoCam. I do this by finding the plane of best fit of the mismatch of the overlapping regions and add this plane to the bottom image. At the end of the stitching process I remove the plane of best fit of the entire image to center it on the middle image. An example of this stitching process can be seen in figure 7a and figure 9a.

To further expand our imaging area we make a least squares fit for our 4 mm $\times$ 7.5 mm image. The defocus and both astigmatic modes are quadratic in nature, which lends them well to a polynomial model. Our model for the mirror surface is,

$$Z(x,y) = a(x-f)^2 + b(x-f)(y-g) + c(y-g)^2 + d, \tag{6}$$

and we are able to omit the linear terms as we can correct for the tip and tilt using mounting stages. The piston term is included in our model to let the center (f, g) have an additional degree of freedom. We can fit the mirror surface to this model and evaluate the accuracy of the model using the R-squared value. Using this method we expand our surface to a 10 mm $\times$ 10 mm area.

3.5 The Matrix Approach

The matrix approach aims to work around the inherit clipped domain of our height map by working in two Hermite Gauss bases. The first of which is the clipped HG basis. These are the coupling coefficients that we calculate from the restricted NanoCam domain. We will get some overlapping into different modes as the Hermite Polynomials are not orthogonal on this scale, more on how to resolve this briefly. The second basis is the full HG basis, which will be the coupling coefficients on an infinite domain. This is what we are ultimately interested in as it is the natural basis for higher order modes which we are concerned about lensing into. We express the conversion between both bases as a matrix equation.

$$\begin{bmatrix} \mathrm{HG}_{\mathrm{clipped},1} \\ \mathrm{HG}_{\mathrm{clipped},2} \\ \vdots \\ \mathrm{HG}_{\mathrm{clipped},n} \end{bmatrix} = \begin{bmatrix} m_{11} & m_{12} & \cdots & m_{1m} \\ m_{21} & m_{22} & \cdots & m_{2m} \\ \vdots & \vdots & \ddots & \vdots \\ m_{n1} & m_{n2} & \cdots & m_{nm} \end{bmatrix} \cdot \begin{bmatrix} \mathrm{HG}_{\mathrm{full},1} \\ \mathrm{HG}_{\mathrm{full},2} \\ \vdots \\ \mathrm{HG}_{\mathrm{full},m} \end{bmatrix} \tag{7}$$

The indexing in equation 7 follows the subsequent pattern for $n + m \leq 3$.

Index	Hermite Gauss Mode
HG_1	HG_{00}
HG_2	HG_{10}
HG_3	HG_{01}
HG_4	HG_{20}
HG_5	HG_{11}
HG_6	HG_{02}
HG_7	HG_{30}
HG_8	HG_{21}
HG_9	HG_{12}
HG_{10}	HG_{03}

Table 1: Indexing for Hermite Gauss Modes. This table demonstrates the indexing pattern for the HG modes for $n + m \leq 3$.

To calculate the M matrix for equation 7, each m_{ij} is defined as the overlap integral of the HG_i and HG_j mode over the restricted NanoCam area. You can then take the inverse of this matrix to convert from $\mathrm{HG}_{clipped}$ to HG_{full}. Note this sometimes requires a pseudoinverse. This matrix then takes into account the non-orthonormality of the Hermite Polynomials on the smaller area by having non-zero non-diagonal entries. This matrix simplifies to the identity matrix as the NanoCam area becomes much greater than the beam spot size.

3.6 Unspoked End Mirror Imaging

The unspoked mirror is a circular silicon mirror that is compressed in an aluminum ring. It has four spokes which we can actuate on. The mode that I have had the most success with so far has been the Xmode. We can see the comparison of the raw and expanded data in figure 7b. Although the Xmode is not perfectly aligned on the y-axis this gives us an estimate to the accuracy of our fitting model, equation 6, and the power we are able to dissipate.

This fit had an R-squared 0.999, indicating a very strong fit and enforces that the majority of the mirror deformations are quadratic. The weighted rms of the residual is 0.79 nm, resulting in the unaccounted residual scattering 0.004% of the total laser power. This was calculated using a formula developed by Robert Nyman and Benjamin Walker for scattering from surface roughness [5],

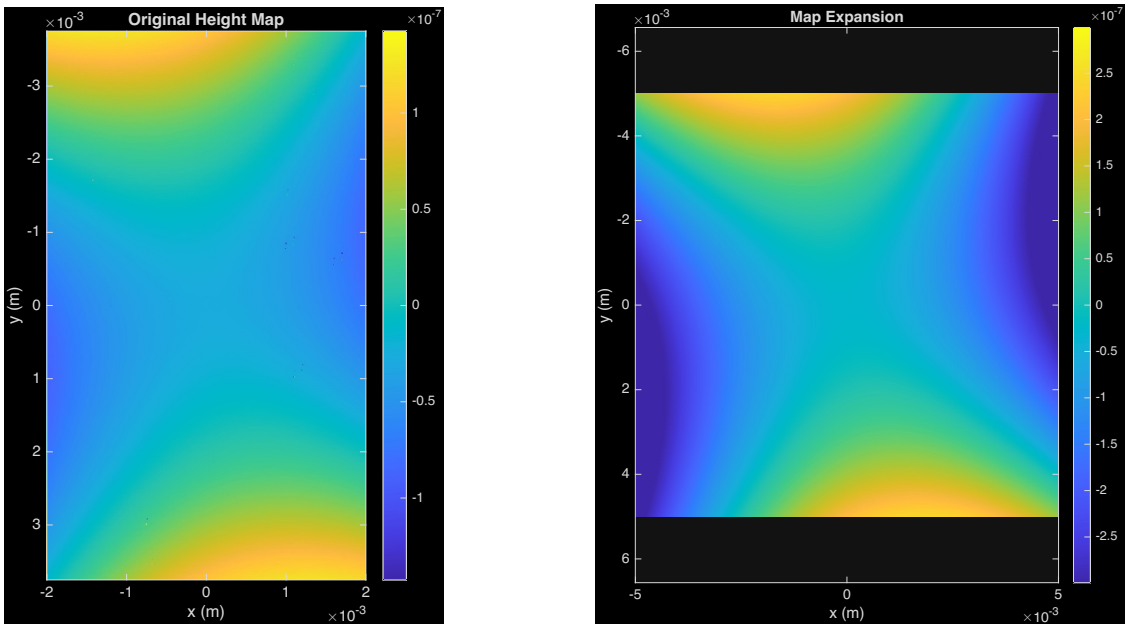

(a) Stitched Difference Map

(b) Expanded Difference Map

Figure 7: XMode Using Stitching and Expansion. In figure 7a we can see the correction on the mirror surface. This is three images stitched together. In figure 7b we can see the expansion of this data using our model, equation 6. This shows the growth from 4 mm × 7.5 mm to 10 mm × 10 mm. R-squared 0.999.

$$P_s = 4k^2\sigma^2 \tag{8}$$

where P_s is the scattered power, k is the laser wave number, and σ is the weighted rms.

As the residual scattering is minimal we can use our expanded map as a strong approximation of the mirror surface and can hence calculate accurate coupling coefficients. The power scattered into the first six Hermite Gauss modes is displayed in table 2.

n prime	m prime	Coupling Coefficient Power
0	0	0.83631
0	1	0.0
1	0	0.0
0	2	0.07128
1	1	0.01598
2	0	0.04272

Table 2: Power Coupling Coefficients from Xmode. This table displays the coupling coefficient data for the Xmode fit, figure 7. We expect to need to correct 2.6×10^{-4} diopters of focusing power and with this configuration we corrected 9.4×10^{-2}.

For GQuEST to reduce the classical noise of the mirror sufficiently we expect to need to

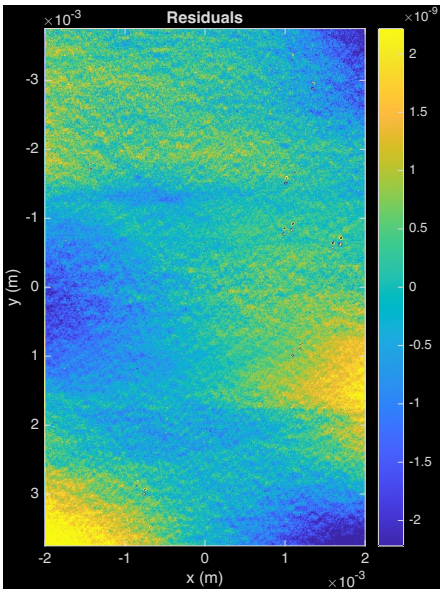

Figure 8: Fitting Residual for Xmode. The residuals of the fit conducted in figure 7. The rms is 1.11 nm and the weighted rms is .788 nm.

correct 2.6×10^{-4} diopters of focusing power. With this configuration we corrected 9.4×10^{-2} diopters. This means we are able to bend the mirror enough to correct for the expected curvature. However, the Xmode should only couple to the HG_{02} and HG_{20} and a significant portion, around 10%, of the power coupled to the HG_{11} mode. We expect to be able to improve the purity of the mirror correction with a spoked mirror. Currently the mirror sits in an aluminum frame that holds and deforms it. We are currently moving to a spoked mirror that has the spokes cut as part of the mirror surface avoiding the aluminum ring.

I have also been able to generate the twist mode on the mirror. To create this mode I twist the spokes attached to the mirror. This causes the mirror to lift on its diagonal. This in contrary to the Xmode where I push down on the spokes to create the saddle shape. Due to the less direct contact on the spokes the twist mode seams to have worse definition, figure 9.

n prime	m prime	Coupling Coefficient Power
0	0	0.99940
0	1	0.0
1	0	0.0
0	2	0.00018
1	1	0.00032
2	0	0.0

Table 3: Power Coupling Coefficients from Twist Mode. This table displays the coupling coefficient data for the twist mode fit, figure 9b. We expect to need to correct 2.6×10^{-4} diopters of focusing power and with this configuration we corrected 4.1×10^{-3}.

The power coupled to each mode is displayed in table 3. The twist mode should only couple to the HG_{11} mode. I was able to correct 4.1×10^{-3} diopters of focusing power but only

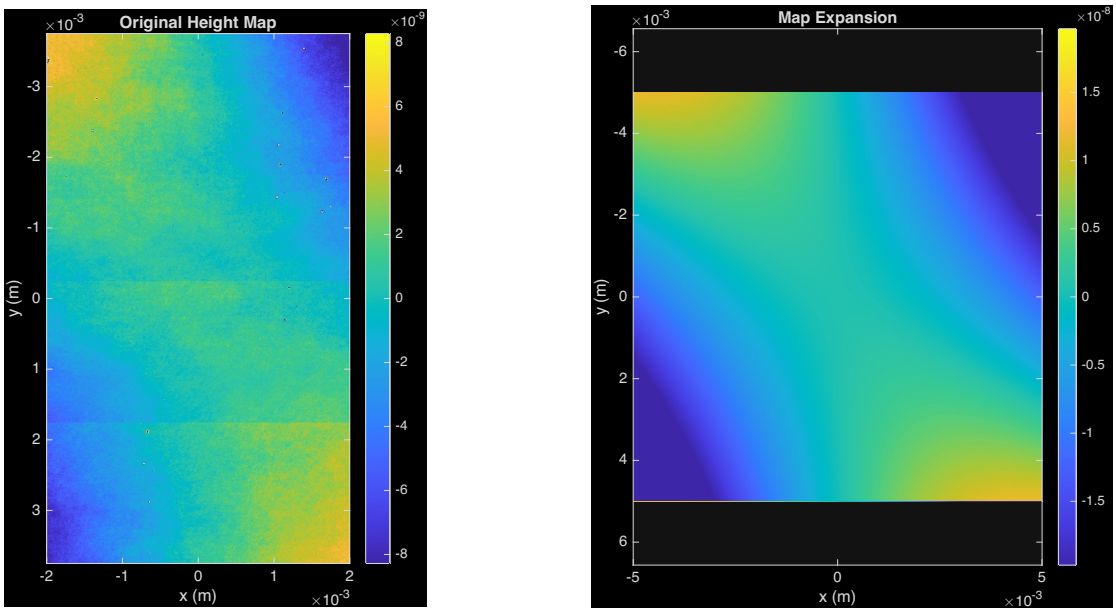

(a) Stitched Difference Map

(b) Expanded Difference Map

Figure 9: Twist Mode Using Stitching and Expansion. In figure 9a we can see the correction on the mirror surface. This is three images stitched together. In figure 9b we can see the expansion of this data using our model, 6. This shows the growth from 4 mm × 7.5 mm to 10 mm × 10 mm. R-squared 0.853.

2.8×10^{-3} diopters are due to the HG_{11}. Again the purity of the correcting power is the primary figure of improvement for the rest of the project. The final mode we are interested in is the Omode (defocus mode). Thus far I have no been able to create a clear Omode, but similar to the purity of the Xmode and twist mode I predict I will be able to create it with the the spoked mirror.

3.7 Spoked End Mirror Imaging

The spoked end mirror is made out of silicon with four spokes. I decided to image the spoked mirror before swapping it for the unspoked end mirror. This would allow us to check if the mount adds any stress to the mirror. GQuEST is considering two types of spoked mirrors, an octagonal barrel and circular barrel spoked mirror. The images of the unmounted mirrors came from stitching a 3×3 grind of images and can be seen in figure 10.

The circular spoked mirror had an rms of 1.87 nm while the octagonal spoked mirror had an rms of 1.14 nm. Because the octagonal mirror appears to be flatter I am choosing to use this mirror for future deformations.

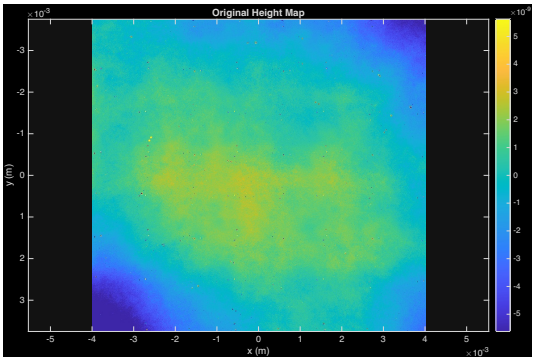

(a) Unmounted Circular Spoked Mirror

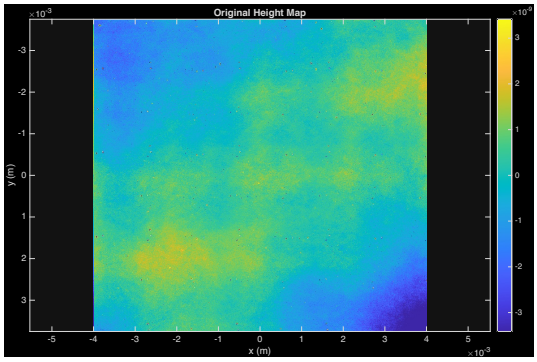

(b) Unmounted Octagonal Spoked Mirror

Figure 10: Unmounted Spoked Mirrors. In figure 10a we can see the height map of the circular spoked mirror, rms = 1.87 nm. In figure 10b we can see the height map of the octagonal spoked mirror, rms = 1.14 nm

.

3.8 Correcting Inherit NanoCam Astigmatism

I found an inherit astigmatism with the NanoCam. I took two images, one of the unstressed unmounted mirror and the same mirror rotated clockwise 90°. I found that the mirrors looking nearly identical (they did not appear to be rotated). After taking multiple pictures I concluded that the NanoCam was adding an offset to the image.

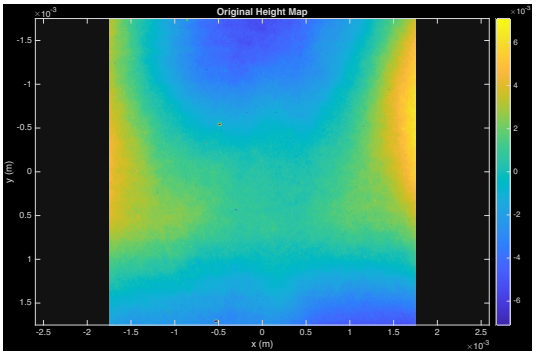

(a) Mirror 0°

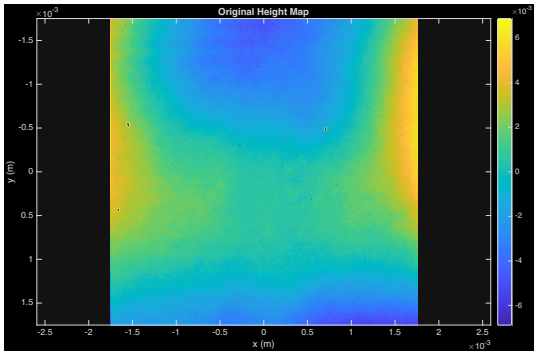

(b) Mirror −90°

Figure 11: Mirror Imaged Aligned and Rotated Clockwise 90°. These images show the offset due to the NanoCam. They should be rotated 90° from each other but they both seam to have the same saddle shape.

One technique to find and correct for this offset is to use a reference flat and subtract the resulting image from future data. I unfortunately didn't have access to reference flat of enough quality and hence devised an algebraic method to correct for the astigmatism.

Suppose we take our two images from figure 11. We can label the image captured of the aligned mirror Z_1 and the image of the 90° rotated mirror Z_2. These images are represented as matrices and are the combination of the mirror surface and NanoCam offset.

$$Z_1 = m_1 + n \tag{9}$$
$$Z_2 = m_2 + n \tag{10}$$

Consider the matrix rotation operation $\hat{r}$, note that this operator is distributive. Because all we did was rotate the mirror we can say that $\hat{r}m_1 = m_2$. We can apply $\hat{r}^{-1}$ to the Z_2 equation and solve the system,

$$\hat{r}^{-1}Z_2 = \hat{r}^{-1}m_2 + \hat{r}^{-1}n \tag{11}$$
$$Z_1 - \hat{r}^{-1}Z_2 = m_1 + n - \hat{r}^{-1}m_2 - \hat{r}^{-1}n \tag{12}$$
$$Z_1 - \hat{r}^{-1}Z_2 = n - \hat{r}^{-1}n \tag{13}$$

We are curious to find the n matrix as this represents the offset of the NanoCam and we know Z_1 and Z_2, note that we have eliminated the m_1 and m_2 terms. The resulting system can be solved using a matrix equation. As an example suppose a smaller 3×3 case with $\hat{r}$ representing a rotation 90° clockwise.

$$n = \begin{bmatrix} n_{11} & n_{12} & n_{13} \\ n_{21} & n_{22} & n_{23} \\ n_{31} & n_{32} & n_{33} \end{bmatrix}, \quad \hat{r}^{-1}n = \begin{bmatrix} n_{13} & n_{23} & n_{33} \\ n_{12} & n_{22} & n_{32} \\ n_{11} & n_{21} & n_{31} \end{bmatrix} \tag{14}$$

$$n - \hat{r}^{-1}n = \begin{bmatrix} n_{11} - n_{13} & n_{12} - n_{23} & n_{13} - n_{33} \\ n_{21} - n_{12} & n_{22} - n_{22} & n_{23} - n_{32} \\ n_{31} - n_{11} & n_{32} - n_{21} & n_{33} - n_{31} \end{bmatrix} \tag{15}$$

This equation can be represented as matrix operation if we reshape n into a column vector.

$$\begin{bmatrix} 1 & 0 & 0 & 0 & 0 & 0 & -1 & 0 & 0 \\ 0 & 1 & 0 & -1 & 0 & 0 & 0 & 0 & 0 \\ -1 & 0 & 1 & 0 & 0 & 0 & 0 & 0 & 0 \\ 0 & 0 & 0 & 1 & 0 & 0 & 0 & -1 & 0 \\ 0 & 0 & 0 & 0 & 0 & 0 & 0 & 0 & 0 \\ 0 & -1 & 0 & 0 & 0 & 1 & 0 & 0 & 0 \\ 0 & 0 & 0 & 0 & 0 & 0 & 1 & 0 & -1 \\ 0 & 0 & 0 & 0 & 0 & -1 & 0 & 1 & 0 \\ 0 & 0 & -1 & 0 & 0 & 0 & 0 & 0 & 1 \end{bmatrix} \begin{bmatrix} n_{11} \\ n_{21} \\ n_{31} \\ n_{12} \\ n_{22} \\ n_{32} \\ n_{13} \\ n_{23} \\ n_{33} \end{bmatrix} \tag{16}$$

Hence if we define $\vec{Z}$ to be the column vector representation of $Z_1 - \hat{r}^{-1}Z_2$ and $\vec{n}$ to be the column vector representation of n then we can solve for $\vec{n}$,

$$\vec{Z} = \begin{bmatrix} 1 & 0 & 0 & 0 & 0 & 0 & -1 & 0 & 0 \\ 0 & 1 & 0 & -1 & 0 & 0 & 0 & 0 & 0 \\ -1 & 0 & 1 & 0 & 0 & 0 & 0 & 0 & 0 \\ 0 & 0 & 0 & 1 & 0 & 0 & 0 & -1 & 0 \\ 0 & 0 & 0 & 0 & 0 & 0 & 0 & 0 & 0 \\ 0 & -1 & 0 & 0 & 0 & 1 & 0 & 0 & 0 \\ 0 & 0 & 0 & 0 & 0 & 0 & 1 & 0 & -1 \\ 0 & 0 & 0 & 0 & 0 & -1 & 0 & 1 & 0 \\ 0 & 0 & -1 & 0 & 0 & 0 & 0 & 0 & 1 \end{bmatrix} \vec{n} \tag{17}$$

From $\vec{n}$ we can reconstruct n. By using sparse matrices this is simple for a computer to solve and reconstruct. The results of this approach for figure 11 are shown below in figure 12.

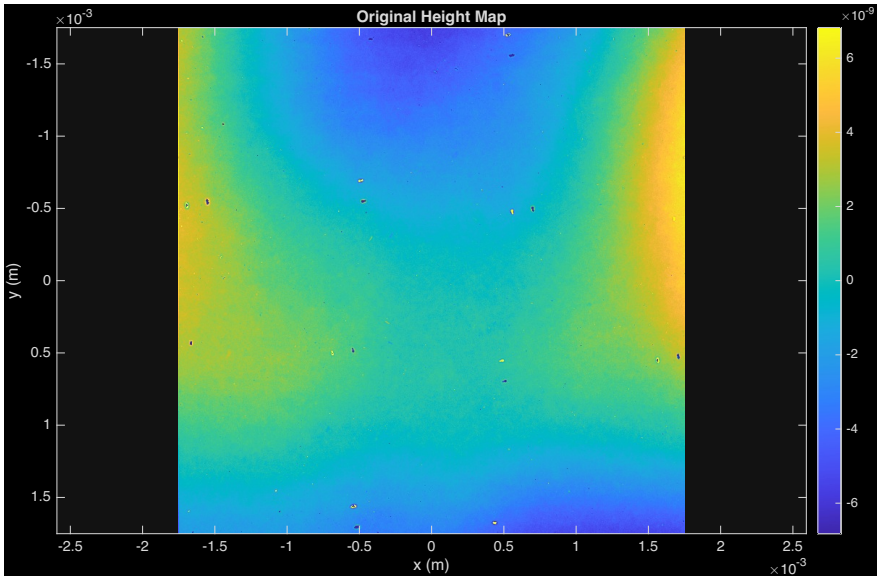

Figure 12: Offset from NanoCam. This is the offset I calculated using the described method from images 11a and 11b. Using this offset the difference between the images had an rms of 0.500 nm while before the difference had an rms of 4.28 nm.

Using the offset to correct both images, the difference between the images had an rms of 0.500 nm while before the correction the difference rms was 4.28 nm.

References

[1]E. P. Verlinde and K. M. Zurek, "Observational signatures of quantum gravity in interferometers", Physics Letters B **822**, 136663 (2021).

[2]S. M. Vermeulen, T. Cullen, D. Grass, I. A. O. MacMillan, A. J. Ramirez, J. Wack, B. Korzh, V. S. H. Lee, K. M. Zurek, C. Stoughton, and L. McCuller, "Photon counting interferometry to detect geontropic space-time fluctuations with GQuEST", Physical Review X **15**, 011034 (2025).

[3] *Zernike polynomials*, in *Wikipedia*, Page Version ID: 1283251556 (Mar. 31, 2025).

[4] *Erin McGee 2024 SURF reports and presentation*, Foswiki, `https://wiki.mccullerlab.com/Main/ErinMcGee2024SURFReportsAndPresentation` (visited on 04/06/2025).

[5] R. A. Nyman and B. T. Walker, *Wave scattering from rough surfaces for good mirrors*, in , arXiv:2005.05201 [physics] (arXiv, May 2020).